Cancer Cell
Article

JunB Protects against Myeloid Malignancies by Limiting Hematopoietic Stem Cell Proliferation and Differentiation without Affecting Self-Renewal

Marianne Santaguida,[1] Koen Schepers,[1] Bryan King,[1] Amit J. Sabnis,[2] E. Camilla Forsberg,[3] Joanne L. Attema,[4] Benjamin S. Braun,[2] and Emmanuelle Passegué[1,*]
[1]The Eli and Edythe Broad Center of Regeneration Medicine and Stem Cell Research, Division of Hematology/Oncology, Department of Medicine
[2]Department of Pediatrics
University of California, San Francisco, San Francisco, CA 94143, USA
[3]Institute for Biology of Stem Cells, University of California, Santa Cruz, Santa Cruz, CA 95064, USA
[4]Institute for Experimental Medical Science, Lund University, 221 84 Lund, Sweden
*Correspondence: passeguee@stemcell.ucsf.edu
DOI 10.1016/j.ccr.2009.02.016

SUMMARY

Loss of the JunB/AP-1 transcription factor induces a myeloproliferative disease (MPD) arising from the hematopoietic stem cell (HSC) compartment. Here, we show that *jun*B inactivation deregulates the cell-cycle machinery and increases the proliferation of long-term repopulating HSCs (LT-HSCs) without impairing their self-renewal or regenerative potential in vivo. We found that JunB loss destabilizes a complex network of genes and pathways that normally limit myeloid differentiation, leading to impaired responsiveness to both Notch and TGF-β signaling due in part to transcriptional deregulation of the *Hes1* gene. These results demonstrate that LT-HSC proliferation and differentiation are uncoupled from self-renewal and establish some of the mechanisms by which JunB normally limits the production of myeloid progenitors, hence preventing initiation of myeloid malignancies.

INTRODUCTION

The mammalian hematopoietic system provides a unique, tractable model for investigating how cancer-associated mutations affect the behavior of specific cell populations and lead to the development of blood cancer or leukemia (Orkin and Zon, 2008). Hematopoietic development is organized hierarchically, starting with a rare population of hematopoietic stem cells (HSCs) that gives rise to a series of committed progenitors and mature cells with particular functional and immunophenotypic properties. HSCs are operationally defined by their ability to provide long-term multilineage reconstitution when transplanted into hematopoietically compromised recipients and are the only cells that self-renew throughout life. HSCs are found predominantly in the bone marrow (BM) associated with several recently described vascular and endosteal niches (Kiel and Morrison, 2008). A complex balance of cell-intrinsic regulators and cell-extrinsic factors present in these niches normally maintain HSCs in a state of relative dormancy and regulate their trafficking to and from these BM niches. Under steady-state conditions, HSCs are a largely quiescent, slowly cycling cell population that, in response to environmental stresses, is capable of dramatic expansion and contraction to ensure proper homeostatic replacement of blood cells (Passegué et al., 2005).

Gene knockout studies in mice have demonstrated that regulation of HSC numbers can be accomplished through direct modulation of HSC proliferative activity, resistance to apoptosis, and retention in the BM niches (Orkin and Zon, 2008). Important

SIGNIFICANCE

Understanding how clonal dominance occurs in the hematopoietic stem cell (HSC) compartment is a central issue in leukemogenesis. Here, we show that inactivation of the JunB transcription factor causes cell-cycle deregulation, disrupts the complex transcriptional network controlling proliferation and differentiation, and decreases responsiveness to Notch and TGF-β signaling. This renders the HSC compartment insensitive to the limits on expansion and myeloid differentiation imposed by those signals. Together, these deregulations lead to the aberrant expansion of myeloid progenitors and myeloproliferative disease development in vivo without causing long-term repopulating HSC (LT-HSC) exhaustion. Our results provide a mechanism explaining how mutations that increase the proliferation of a single LT-HSC can become dominant and lead to the expansion of an aberrant clone within the otherwise normal HSC compartment.

mediators of these processes include cell-cycle regulators such as the D cyclins and the cyclin-dependent kinase inhibitors (CKIs) p21/CIP1 and p18/INK4c. Recent studies have also highlighted the roles of specific signal transducers (Pten), transcription factors (Gfi1, HoxB4, HoxA9), and extrinsic regulatory pathways (Notch, TGF-β, Wnt) in controlling HSC self-renewal and proliferation (Akala and Clarke, 2006; Blank et al., 2008). However, the precise molecular circuitry controlling HSC fate decisions has yet to be fully elucidated, and the mechanisms by which HSC maintenance, proliferation, and differentiation are coordinately regulated to ensure homeostatic production of blood cells remain poorly understood. Recently, it has been suggested that changes in the quiescence status of HSCs (Holyoake et al., 1999) and deregulation of their interaction with BM niches (Jin et al., 2006) could be key events for their leukemic transformation and the development of myeloid leukemia. Still, little is known about the impact of leukemic transformation on HSC biological function and how abnormal HSC-derived leukemia-initiating stem cells (LSCs) differ from normal HSCs.

Originally discovered in leukemia, cancer-initiating stem cells have now been recognized in a variety of solid tumors (Wang and Dick, 2005). They represent a subset of a heterogeneous cancer population and are operationally defined by their ability to drive the formation and growth of a new tumor in transplanted mice. Convincing evidence indicates that LSCs are inefficiently eliminated by current therapeutic treatments and suggests that LSC persistence could be responsible for disease maintenance and/or recurrence (Jordan et al., 2006). Developing therapeutic interventions that specifically target LSCs, an appealing strategy for improving leukemia treatment, requires an understanding of how LSCs escape normal regulatory mechanisms and become malignant. Few mouse models of human leukemia are currently available in which the LSC population has been identified and can be purified for analysis (Wang and Dick, 2005). This is an essential prerequisite for identifying pathways and molecules available for interventional therapies in patients.

We have previously developed several mouse strains lacking the JunB/AP-1 transcription factor that accurately recapitulate important clinical aspects of human myeloid malignancies, including chronic myelogenous leukemia (CML) (Passegué et al., 2001). We have also identified the LSC population as arising from the HSC compartment during the precancerous myeloproliferative disease (MPD) phase (Passegué et al., 2004). Importantly, *jun*B inactivation has been observed in a spectrum of human myeloid malignancies, including CML (Yang et al., 2003), and downregulation of *jun*B expression has been found in the HSC compartment of patients with acute myeloid leukemia (Steidl et al., 2006). At present, little is known about the role of JunB in HSC biology and myeloid leukemia development. Here, we used *jun*B-deficient mice as a model system to understand how JunB normally controls HSC functions and to identify the deregulated mechanisms that are responsible for HSC transformation into LSCs.

RESULTS

Defects in Hematopoietic Reconstitution

To evaluate the impact of *jun*B loss on HSC function in hematopoietic reconstitution, we first performed competitive BM transplantation experiments (Figure 1A). Control and *jun*B-deficient BM cells (1×10^6 total) were mixed in a 1:1 or 9:1 ratio with GFP-expressing competitor BM cells and injected into lethally irradiated recipients. Regardless of the donor/competitor ratio used, we found that *jun*B-deficient BM cells consistently displayed ~50% reduced engraftment efficiency compared to control BM cells. We then directly transplanted 1×10^6 control or *jun*B-deficient BM cells into lethally or sublethally irradiated recipients (Figure 1B and data not shown). While transplantation into lethally irradiated mice yielded comparable reconstitution levels (Passegué et al., 2004), transplantation into sublethally irradiated mice revealed extremely variable engraftment levels, with *jun*B-deficient BM cells being on average 50% less efficient than control BM cells. To confirm the limited engraftment of *jun*B-deficient cells, we transplanted small numbers of an HSC-enriched population (defined as $Flk2^-/Lin^-/Sca\text{-}1^+/c\text{-}Kit^+$ or $Flk2^-$ LSK BM cells, hereafter referred to as hematopoietic stem and progenitor cells [HSPCs]) together with 3×10^5 unfractionated helper BM cells into lethally irradiated recipients (Figure 1C; see also Table S1 available online). While no engraftment was observed after injection of 50 to 100 *jun*B-deficient HSPCs, transplantation of 250 *jun*B-deficient HSPCs resulted in a 2- to 10-fold decrease in reconstitution levels depending mainly upon the use of Sca-1-depleted (HSC-purged) helper BM cells. In every case in which *jun*B-deficient HSPCs engrafted (even at low levels), we observed progressive expansion of the myeloid lineage, leading by 6 to 12 months posttransplantation to the development of an MPD (Figure 1D) similar to the disease observed in primary *jun*B-deficient mice (Passegué et al., 2004).

The engraftment process requires that transplanted HSCs home to the BM cavity and cross the endothelial layer forming the wall of the blood vessels (Lapidot et al., 2005). To assess whether *jun*B-deficient HSPCs are defective in BM homing, we performed short-term in vivo homing assays by injecting lethally irradiated recipients with GFP^+ $Flk2^-$ LSK cells or LSK cells isolated from *jun*B-deficient mice crossed to β-actin GFP transgenic mice. Analysis of peripheral blood (PB), BM, spleen, and the hematopoietic component of the liver for the presence of GFP^+ cells at 3 or 12 hr postinjection revealed similar numbers of control and *jun*B-deficient HSPCs in all tissues, including BM, at both time points (Figure 1E and data not shown). We also used intrafemoral injections of 1×10^6 BM cells into sublethally irradiated recipients to confirm that impaired homing did not contribute to the reduced engraftment of *jun*B-deficient cells (Figure 1F; Figure S1). Taken together, these results indicate that despite normal lodging in the BM cavity after transplantation, *jun*B-deficient HSPCs are impaired in their ability to engraft in the BM niches and to contribute to hematopoietic reconstitution. This suggests either that *jun*B-deficient HSCs are defective in BM maintenance or that fewer long-term repopulating HSCs (LT-HSCs) are present in the transplanted *jun*B-deficient populations.

Deregulated Cell-Cycle Distribution

HSC engraftment following transplantation as well as maintenance during steady-state hematopoiesis critically depends upon their quiescent state (Passegué et al., 2005). We next investigated whether the engraftment defects observed with *jun*B-deficient HSPCs could result from changes in their

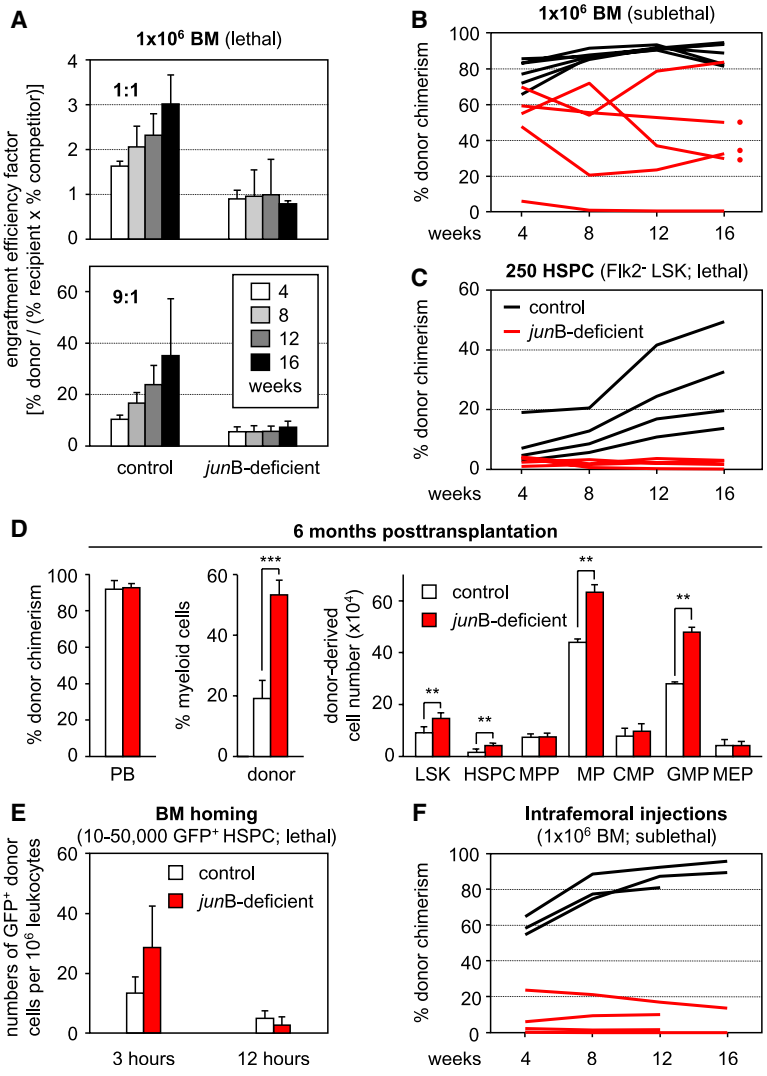

Figure 1. Hematopoietic Reconstitution Potential and Homing Activity of *junB*-Deficient Bone Marrow Cells

Lethally or sublethally irradiated recipients (CD45.1) were transplanted with the indicated number and type of donor control or *junB*-deficient cells (CD45.2). Mice were bled every 4 weeks and analyzed for % CD45.2 chimerism in the peripheral blood (PB).

(A) Transplantation of 1 × 10^6 unfractionated bone marrow (BM) cells (1:1 and 9:1 ratio of donor and competitor GFP$^+$/CD45.1 cells) into lethally irradiated recipients (n = 5 mice per cohort). Engraftment efficiency factor (percentages ± SD) was calculated as ([% CD45.2$^+$ donor cells]/[(% CD45.1$^+$ recipient and competitor cells) × (% GFP$^+$ competitor cells)]).

(B) Transplantation of 1 × 10^6 unfractionated BM cells into sublethally irradiated recipients (n = 5 mice per cohort).

(C) Transplantation of 250 purified hematopoietic stem and progenitor cells (HSPCs: Flk2$^-$ LSK) together with 3 × 10^5 helper CD45.1 BM cells into lethally irradiated recipients (n = 4 mice per cohort).

(D) Myeloproliferative disease (MPD) development in recipients of *junB*-deficient BM cells (red dots in [B]). The % CD45.2 chimerism and donor-derived myeloid (Gr-1$^+$/Mac-1$^+$) cells in PB and the total cell numbers for the indicated BM subpopulations are given at 6 months posttransplantation (averages ± SD; n = 3 mice per cohort; **p ≤ 0.01, ***p ≤ 0.001). MPP, multipotent progenitors (Flk2$^+$ LSK); MP, myeloid progenitors (Lin$^-$/Sca-1$^-$/c-Kit$^+$); CMP, common myeloid progenitors; GMP, granulocyte/macrophage progenitors; MEP, megakaryocyte/erythrocyte progenitors.

(E) Short-term in vivo homing assay. Sublethally irradiated recipients (n = 3 mice per cohort) were injected with either 50,000 LSK cells (3 hr) or 10,000 Flk2$^-$ LSK cells (12 hr) isolated from β-actin GFP control and *junB*-deficient mice. The number (averages ± SD) of transplanted GFP$^+$ cells present in the BM was determined at 3 or 12 hr postinjection.

(F) Intrafemoral injections. 1 × 10^6 unfractionated BM cells were injected directly into the femoral cavity of sublethally irradiated recipients (one femur injected per mouse, n = 3–4 mice per cohort).

cell-cycle distribution. Analyses performed using either live Hoechst 33342 (H)/pyronin Y (PY) staining on purified Flk2$^-$ LSK cells or intracellular 7-aminoactinomycin D (7AAD)/PY staining on unfractionated BM cells (Figure 2A; Table S2) revealed that *junB*-deficient HSPCs had on average a 2-fold decrease in the percentage of quiescent G_0 cells and a correlative increase in the percentage of cycling G_1 and S-G_2/M cells. Short-term kinetic analysis of bromodeoxyuridine (BrdU) incorporation indicated increased proliferation rates in *junB*-deficient HSPCs, with ~13% of BrdU$^+$ cells after 1 hr incorporation reaching 24% after 12 hr compared to ~8% and ~19%, respectively, for control HSPCs (Figure 2B and data not shown). Ki-67 and phosphohistone H3 immunofluorescence staining on isolated Flk2$^-$ LSK cells further confirmed that *junB*-deficient HSPCs have a higher proliferative index (Table S2).

To understand the deregulations occurring at the molecular level, we used quantitative RT-PCR (qRT-PCR) to analyze the expression level of a comprehensive panel of cell-cycle genes in Flk2$^-$ LSK cells isolated from pools of control mice (3–5 mice) or from age-matched individual *junB*-deficient mice (Figure 2C). Although significant fluctuations in gene expression were observed between the individual *junB*-deficient HSPC populations (likely reflecting differences in the stage of MPD development in the respective donor mice), we found a consistent decrease in the expression levels of early G_1 cyclins (mainly *D1*) and of two CKIs (*p18* and *p57*), associated with a trend toward increased expression of late G_1 cyclins (*E1* and *E2*) and S-G_2/M cyclins (*A2* and *F*). Furthermore, we confirmed a decrease in cyclin D1 protein levels in *junB*-deficient HSPCs using intracellular fluorescence-activated cell sorting (FACS) analysis (Figure 2D). Taken together, these results provide a molecular signature of the deregulations occurring in the cell-cycle regulation of *junB*-deficient HSPCs and a mechanism for their enhanced proliferation.

Quiescence Status and Engraftment Potential

Increased proliferation and altered ratios of quiescent versus cycling HSPCs may indicate that the engraftment defect observed with *junB*-deficient cells results from transplanting fewer numbers of quiescent HSCs. To test this hypothesis, Flk2$^-$ LSK cells were isolated, stained with H/PY, and re-sorted for the G_0 subset, after which 250 G_0 HSPCs were transplanted

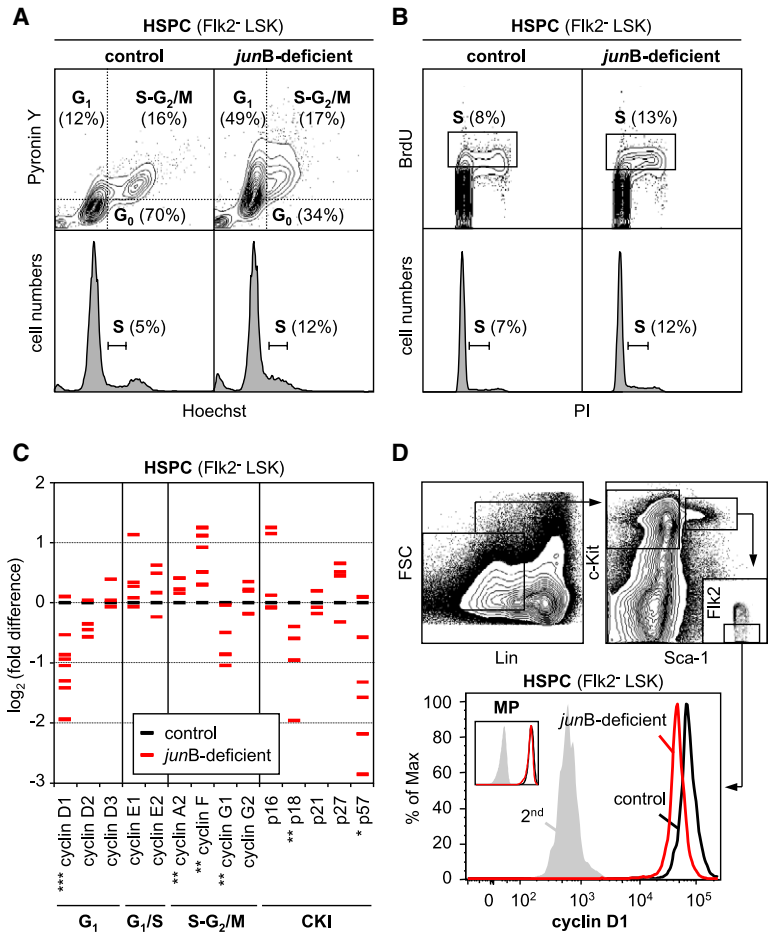

Figure 2. Deregulated Proliferation and Regulation of the Cell-Cycle Machinery in *jun*B-Deficient HSPCs

(A) Live Hoechst (H)/pyronin Y(PY) staining of purified control and *jun*B-deficient HSPCs. Quiescent G_0 cells are H^{2n}/PY^- while proliferative G_1 and S-G_2/M cells are H^{2n}/PY^+ and $H^{\geq 2n-4n}/PY^+$, respectively. Bottom histograms indicate DNA content.

(B) BrdU incorporation (1 hr in vivo pulse) in purified control and *jun*B-deficient HSPCs. Cells in S phase (boxed) are $BrdU^+$ and have $\geq$2n DNA content as determined by propidium iodide (PI) counterstaining (bottom histograms).

(C) Quantitative RT-PCR analysis of cell-cycle gene expression in control and *jun*B-deficient HSPCs. $Flk2^-$ LSK cells were isolated from pools of 3–5 control mice and from age-matched individual *jun*B-deficient mice. The results shown are averages of triplicate measurements and are expressed as $\log_2$(fold difference) compared to the levels found in control HSPCs ($^*p \leq 0.05$, $^{**}p \leq 0.01$, $^{***}p \leq 0.001$; β-*actin* normalization). For each gene, 3–9 independent samples were analyzed per genotype (some red dashes are overlapping).

(D) Intracellular fluorescence-activated cell sorting (FACS) analysis of cyclin D1 protein levels in control and *jun*B-deficient HSPCs and myeloid progenitors (MP: $Lin^-/Sca\text{-}1^-/c\text{-}Kit^+$).

into lethally irradiated recipients together with a radioprotective dose of Sca-1-depleted helper BM cells (Figure 3A). Surprisingly, we found that *jun*B-deficient G_0 HSPCs still displayed severe defects in hematopoietic reconstitution compared to the same number of control G_0 HSPCs. This result prompted our reevaluation of the cell surface marker combination used to identify engrafting HSCs by performing intracellular 7AAD/PY staining for cell-cycle distribution together with additional molecules that enrich for LT-HSC activity: CD34 (Osawa et al., 1996) and the signaling lymphocyte attractant molecule (SLAM) markers CD150 and CD48 (Kiel et al., 2005). As expected, using the CD34 marker we identified a highly quiescent $CD34^-/Flk2^-$ LSK population in control mice (Figure S2). However, in the *jun*B-deficient mice, the $CD34^-/Flk2^-$ LSK cells also displayed aberrant cell-cycle distribution with massive recruitment into G_1 and significant expansion in numbers. In sharp contrast, using the SLAM markers, we identified a highly quiescent $CD150^+/CD48^-/Flk2^-$ LSK population (G_0, 92.4% ± 3.5% versus 89.5% ± 3.8%; G1-S-G_2/M, 2.2% ± 2.3% versus 10.5% ± 4.1%; n = 5) that was of similar size in both control and *jun*B-deficient mice (Figures 3B and 3C). This staining strategy also revealed that the increase in size of the *jun*B-deficient HSPC compartment was caused almost entirely by an increase in $CD48^+/Flk2^-$ LSK cells (Figure 3B).

Subsequently, we transplanted 250 $CD150^+/CD48^-/Flk2^-$ LSK or $CD48^+/Flk2^-$ LSK cells into lethally irradiated recipients to investigate their engraftment potential (Figure 3D). As expected, neither control nor *jun*B-deficient $CD48^+/Flk2^-$ LSK cells provided long-term reconstitution (Kiel et al., 2005). In fact, $CD48^+/Flk2^-$ LSK cells only gave rise to a transient myeloid readout without long-lasting lymphoid cell production (data not shown), and their progenies were almost completely absent from the recipient mice at 1 month posttransplantation (Figure 3D). Strikingly, *jun*B-deficient $CD150^+/CD48^-/Flk2^-$ LSK cells displayed quantitatively enhanced and more robust repopulating activity than control cells, which reflects their increased production of mature myeloid cells. By 11 months posttransplantation, robust and sustained engraftment was observed in both cohorts (control, 78% ± 14% chimerism; *jun*B-deficient, 93% ± 2% chimerism; n = 5), accompanied by MPD development in mice transplanted with *jun*B-deficient cells (data not shown). Taken together, these results demonstrate that $CD150^+/CD48^-/Flk2^-$ LSK cells are the true quiescent and engrafting LT-HSCs in both control and *jun*B-deficient mice. They also indicate that the reconstitution defects observed upon transplantation of *jun*B-deficient unfractionated BM or purified HSPCs result from dilution of these engrafting LT-HSCs by the expanded, nonengrafting $CD48^+/Flk2^-$ LSK cells. Furthermore, they provide an explanation for the puzzling outcome of the G_0 HSPC transplantation experiments (Figure 3A) since the transplanted *jun*B-deficient G_0 HSPCs contained a much larger fraction of nonengrafting G_0 $CD48^+/Flk2^-$ LSK cells (Figure S3) than control G_0 HSPCs, hence again diluting the true engrafting quiescent LT-HSCs.

Increased Proliferation with Normal Regenerative Potential

Next, we tested whether *jun*B-deficient LT-HSCs, despite maintaining normal numbers in the BM, could have increased

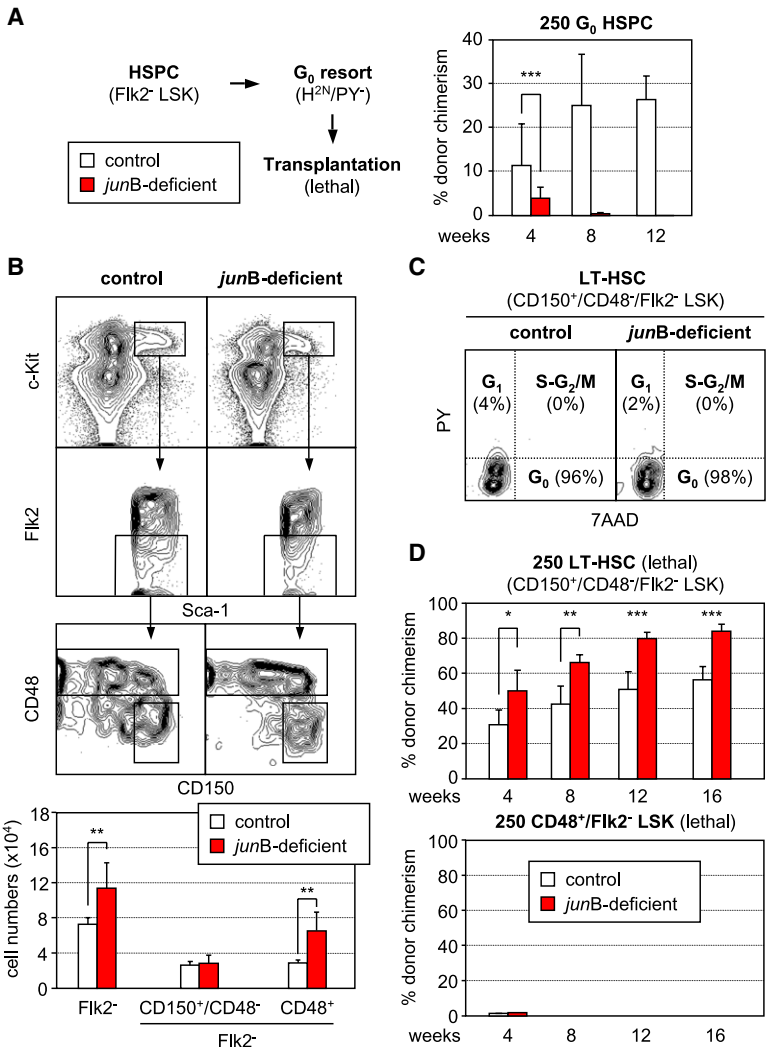

Figure 3. Persistence of a Highly Quiescent Long-Term Repopulating Hematopoietic Stem Cell Population with Normal Engraftment Potential in *junB*-Deficient Mice

(A) Hematopoietic reconstitution from quiescent HSPCs. Flk2$^-$ LSK cells were isolated from control and *junB*-deficient mice (CD45.2), stained with H/PY, and re-sorted for the G_0 (H^{2n}/PY$^-$) subpopulation. Lethally irradiated recipient mice (CD45.1; n = 3 per cohort) were injected with 250 purified G_0 HSPCs together with 3 × 10^5 Sca-1-depleted helper CD45.1 BM cells and analyzed monthly for percentages (±SD) of CD45.2 chimerism in PB (***p ≤ 0.001).

(B) SLAM marker subfractionation of the HSPC compartment in control and *junB*-deficient mice. The FACS plots show examples of CD150 and CD48 expression in the Flk2$^-$ LSK compartment, and the bottom graph summarizes the total numbers (averages ± SD) of Flk2$^-$ LSK and SLAM subsets in control (n = 7) and *junB*-deficient (n = 5) mice (**p ≤ 0.01).

(C) Cell-cycle analysis of CD150$^+$/CD48$^-$/Flk2$^-$ LSK cells in control and *junB*-deficient mice. BM cells were stained for CD150 expression in the Flk2$^-$ LSK compartment (with CD48 included in the lineage cocktail; see Figure S3) in combination with intracellular staining for cell-cycle distribution (7-aminoactinomycin D [7AAD]/PY). Quiescent G_0 cells are 7AAD^{2n}/PY$^-$ while proliferative G_1 and S-G_2/M cells are 7AAD^{2n}/PY$^+$ and 7AAD$^{\geq 2n-4n}$/PY$^+$, respectively.

(D) Hematopoietic reconstitution from CD150$^+$/CD48$^-$/Flk2$^-$ LSK and CD48$^+$/Flk2$^-$ LSK subsets. Cells were isolated from CD45.2 control and *junB*-deficient mice, and 250 cells for each subset were injected together with 3 × 10^5 Sca-1-depleted helper CD45.1 BM cells into lethally irradiated CD45.1 recipients. Mice (n = 5 per cohort) were analyzed every 4 weeks for % (±SD) CD45.2 chimerism in PB (*p ≤ 0.05, **p ≤ 0.01, ***p ≤ 0.001).

proliferation rates using long-term BrdU incorporation as described recently (Kiel et al., 2007) (Figure 4A; Table S3). Control and *junB*-deficient mice were injected intraperitoneally with BrdU (1 mg/6 g body weight) and then fed BrdU (1 mg/ml) in their drinking water for up to 10 days. LT-HSCs (CD150$^+$/CD48$^-$/Flk2$^-$ LSK cells) were isolated, and the cells that incorporated BrdU while replicating their DNA were enumerated by immunofluorescence analysis. In addition, we also quantified BrdU incorporation by intracellular FACS analysis (Figure S4). Using both detection methods, we found that *junB*-deficient LT-HSCs displayed significantly increased BrdU incorporation compared to control LT-HSCs, reaching 60.7% ± 2.5% versus 42.5% ± 0.7% (n = 4; p ≤ 0.005) after 10 days of BrdU administration. Cell-cycle entry rates, calculated by regression on the log of the proportion of unlabelled cells (Cheshier et al., 1999), revealed that ~13.6% of *junB*-deficient LT-HSCs entered the cell cycle each day (with a population doubling time of 16.3 days), compared to only ~6.4% per day for control LT-HSCs (with a population doubling time of 26.9 days). We also performed qRT-PCR analysis for the expression of quiescence- and cell-cycle-associated genes in *junB*-deficient LT-HSCs (Figure 4B). Interestingly, we found a significant increase in the expression level of G_0/G_1 transition kinase cyclin C together with changes already observed in *junB*-deficient HSPCs, mainly decreased expression of the CKIs *p18*, *p57*, and *cyclin D1* and increased expression of the mitotic *cyclin A2*.

The increased proliferation of *junB*-deficient LT-HSCs raised the possibility that these cells might exhaust faster than normal LT-HSCs under regenerative stress conditions, as suggested by other studies using transplantation of more or less purified cell populations (Orford and Scadden, 2008). To address this question without using the transplantation system, we evaluated hematopoietic recovery and survival after serial injections of the myelosuppressive agent 5-fluorouracil (5-FU; 150 mg/kg) (Figure 4C). When 5-FU was injected every second month (to allow complete recovery between injections), both control and *junB*-deficient mice started dying by the third 5-FU injection without any significant difference between the two groups. As expected, *junB*-deficient mice always displayed higher restoration levels of the myeloid lineage than control mice, indicating constant regeneration of the MPD from *junB*-deficient LT-HSCs that persisted after 5-FU treatment. When 5-FU was injected every 7 days (to continuously deplete regenerating progenitor populations), both control and *junB*-deficient mice also displayed similar survival rates, with the majority of deaths

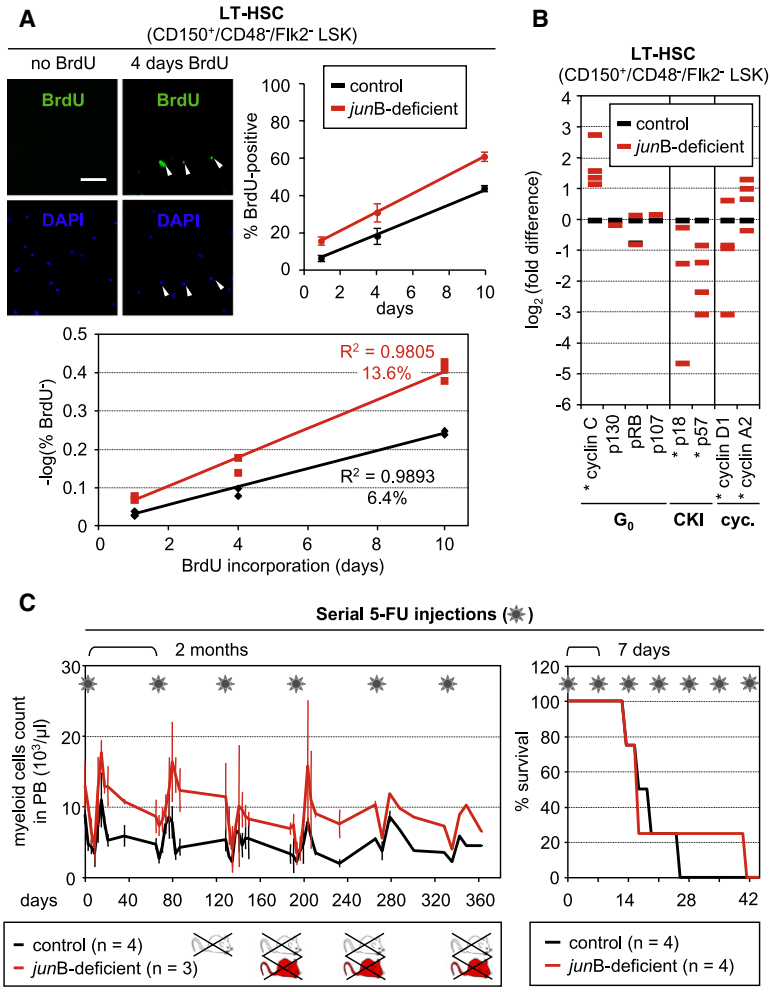

Figure 4. Deregulated Turnover Rates but Normal Regeneration Potential in *junB*-Deficient Long-Term Repopulating Hematopoietic Stem Cells

(A) Long-term kinetics of BrdU incorporation in long-term repopulating hematopoietic stem cells (LT-HSCs). CD150$^+$/CD48$^-$/Flk2$^-$ LSK cells were isolated from individual control and *junB*-deficient mice fed with BrdU for the indicated number of days (n = 2–3 mice per time point). Images show representative examples of BrdU staining (scale bar = 100 mm; arrowheads indicate BrdU$^+$ LT-HSCs). BrdU enumeration upon immunofluorescence detection (upper right; averages ± SD) and calculation of the regression on the log of the proportion of unlabeled cells (bottom) are also shown.

(B) Quantitative RT-PCR analysis of cell-cycle gene expression in control and *junB*-deficient LT-HSCs. CD150$^+$/CD48$^-$/Flk2$^-$ LSK cells were isolated from pools of age-matched control and *junB*-deficient mice (2–3 mice per pool, n = 3). Results shown are averages of triplicate measurements and are expressed as $\log_2$(fold difference) compared to the levels found in control LT-HSCs (*p $\leq$ 0.05; β-*actin* normalization).

(C) Serial 5-fluorouracil (5-FU) injections. Control and *junB*-deficient mice were injected intraperitoneally with 150 mg/kg 5-FU (asterisks) either every 2 months or every 7 days. For the 2-month protocol (left), the kinetics of myeloid recovery following 5-FU injection were evaluated. The results (averages ± SD) show myeloid cell counts in PB as assessed by automated complete blood count (CBC). For the 7-day protocol (right), survival rates postinjection were determined.

occurring by the third or fourth 5-FU injection. These results indicate that *junB*-deficient LT-HSCs have regenerative potential similar to, and do not exhaust faster than, control LT-HSCs. Taken together with the transplantation data, these data demonstrate that the fast-cycling *junB*-deficient LT-HSCs have normal self-renewal activity in vivo.

Broad Transcriptional Deregulations

To determine how loss of JunB affects HSC fate decisions, we first analyzed *junB*-deficient HSPCs by qRT-PCR for the expression levels of genes known to play a role in self-renewal, quiescence, proliferation regulation, and oncogenic transformation (Figure 5A). Overall, we found a general trend toward decreased gene expression in *junB*-deficient Flk2$^-$ LSK cells, with significant reductions in the levels of *Pten*, *Hoxb4*, and *Hoxa9* (self-renewal genes) and *Notch1*, *Hes1*, and *Hes5* (Notch pathway genes); nonsignificant reductions in N-*myc* and c-*Myb* (oncogenes); and no changes in cell-cycle regulators and TGF-β pathway components. To exclude measuring changes reflecting only the expansion of the CD48$^+$/Flk2$^-$ LSK cells observed in *junB*-deficient mice, we also analyzed the expression of the self-renewal genes in LT-HSCs (Figure 5B). While *Pten*, *Hoxb4*, *Hoxa9*, and *Notch1* did not exhibit significant changes in quiescent *junB*-deficient LT-HSCs, the expression of *Hes1* (a key downstream mediator of both Notch and TGF-β pathways) (Blokzijl et al., 2003) remained significantly decreased. Furthermore, preliminary chromatin immunoprecipitation (ChIP) analysis in wild-type HSPCs and detailed promoter studies in 3T3 fibroblasts identified two repeated JunB binding sites in the proximal region of the mouse *Hes1* promoter and demonstrated that JunB was a direct transcriptional activator of *Hes1* expression (Figure S5).

To functionally assess the status of the Notch pathway in *junB*-deficient HSCs, we performed a short-term coculture experiment on control OP9 stromal cells or OP9 stromal cells expressing the Notch ligand Delta-1 (OP9DL1). Control and *junB*-deficient HSPCs were sorted directly into a 96-well plate containing either OP9 or OP9DL1 cells, grown for 48 hr with or without γ-secretase inhibitor (γ-SI) to prevent activation of the Notch pathway, and analyzed by qRT-PCR for *Hes1* expression levels (Figure 5C). When cultured on OP9DL1 cells, control HSPCs displayed a strong induction of *Hes1* expression that was completely abrogated upon γ-SI treatment. In contrast, *Hes1* expression was not significantly induced in *junB*-deficient HSPCs cultured on OP9DL1 cells, which demonstrated a defective response to Notch stimulation in these cells. We also confirmed defective induction of *Hes1* expression in *junB*-deficient LT-HSCs cocultured for 48 hr on OP9DL1 cells (Figure 5C). To assess the status of the TGF-β pathway, we incubated sorted control and *junB*-deficient HSPCs for 8 hr with recombinant TGF-β and measured by qRT-PCR the expression levels of three direct transcriptional targets of this pathway: *Smad7*, the CKI *p57*, and *Hes1* (Figure 5D). We found

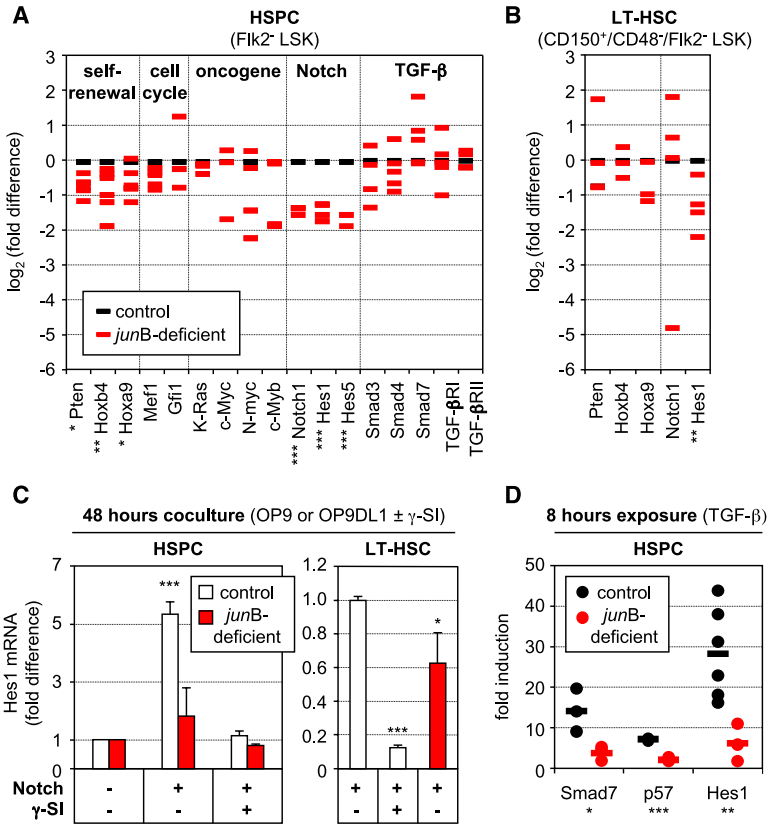

Figure 5. Broad Deregulation of Self-Renewal and Extracellular Signaling Pathway Genes in *jun*B-Deficient LT-HSCs

(A) Quantitative RT-PCR analysis of the expression levels of genes and pathways controlling HSC fate decisions in control and *jun*B-deficient HSPCs. The same cDNA samples used in Figure 2C were used for this analysis (*p ≤ 0.05, **p ≤ 0.01, ***p ≤ 0.001).

(B) Quantitative RT-PCR analysis of control and *jun*B-deficient LT-HSCs. The same cDNA samples used in Figure 4B were used for this analysis (*p ≤ 0.05, **p ≤ 0.01).

(C) Control or *jun*B-deficient HSPCs or LT-HSCs (3,000 cells per well) were directly sorted into 96-well plates containing either OP9 (Notch$^-$) or OP9DL1 (Notch$^+$) cells and incubated for 48 hr with or without γ-secretase inhibitor (γ-SI; 10 μM). The data shown for each population are the averages ± SD of two independent experiments each performed in triplicate (*p ≤ 0.05, ***p ≤ 0.001; β-*actin* normalization). HSPC results are expressed as fold increase compared to *Hes1* levels in control or *jun*B-deficient cells cocultured on OP9 cells without γ-SI (arbitrarily set to 1). LT-HSC results are expressed as fold decrease compared to *Hes1* levels in control cells cocultured on OP9DL1 cells without γ-SI (arbitrarily set to 1).

(D) Control or *jun*B-deficient HSPCs (3,000–20,000 cells per well) were directly sorted into 96-well plates, rested overnight, and stimulated with 5 ng/ml TGF-β for 8 hr. The results are expressed as fold increase compared to *Smad7*, *p57*, and *Hes1* levels found in nonstimulated HSPCs incubated for the same length of time. Independent measurements (each performed in triplicate) from 3–6 experiments and averages (bars) are shown (*p ≤ 0.05, **p ≤ 0.01, ***p ≤ 0.001; *RL-19* normalization).

significantly reduced induction of all three genes in *jun*B-deficient HSPCs compared to control HSPCs, indicating that these cells are also defective in their response to TGF-β stimulation. Taken together, these results indicate that loss of JunB destabilizes a broad network of interconnected genes and pathways that regulate HSC fate decisions and demonstrate that JunB is essential to control the extent to which HSCs respond to Notch and TGF-β stimulation, due in part to JunB involvement in the transcriptional regulation of the common downstream effector gene *Hes1*.

Increased Myeloid Differentiation in Response to Impaired Notch and TGF-β Regulations

Finally, we asked whether the defective response of *jun*B-deficient HSCs to Notch and TGF-β stimulation could contribute to the increased myelopoiesis observed in *jun*B-deficient mice. To answer this question, control and *jun*B-deficient HSPCs and LT-HSCs were first cocultured for 4 days on OP9 or OP9DL1 cells in the presence or absence of TGF-β (Figure 6A). This initial step was designed to assess growth in response to activation of Notch and TGF-β pathways, similar to what is likely provided by the BM niches in vivo. Control cells were also treated with γ-SI and TGF-β inhibitor (T-βI; 5 μM) to mimic the dual impairment observed in *jun*B-deficient HSPCs. After 4 days of coculture, these HSPC- or LT-HSC-derived cells were transferred into methylcellulose containing a cocktail of myeloid cytokines and growth factors (but devoid of TGF-β or inhibitors) to assess myeloid colony-forming activity (CFU). This second step allowed us to estimate the numbers of myeloid progenitors generated in each coculture condition. As expected, stimulation with TGF-β and activation of the Notch pathway (alone or in combination) severely limited growth and myeloid differentiation from control cells compared to untreated cultures (Figures 6B and 6C). In contrast, similar treatments did not significantly inhibit *jun*B-deficient HSPC or LT-HSC expansion rates. Most strikingly, neither Notch induction nor TGF-β stimulation was able to limit myeloid differentiation from *jun*B-deficient cells, which matched the myeloid differentiation potential obtained in untreated cultures (Figures 6B and 6C). Similarly, pharmacological inhibition of Notch and TGF-β signaling in control HSPCs or LT-HSCs partially prevented the growth inhibition and fully relieved the block in myeloid differentiation imposed by these regulatory mechanisms. Taken together, these results indicate that Notch and TGF-β cooperate to limit the rate at which LT-HSCs and early progenitor cells expand (via both pathways) and differentiate (mostly via TGF-β) to produce myeloid progenitors. They also suggest that lack of response to Notch and TGF-β contributes to the ability of *jun*B-deficient LT-HSCs to constitutively overproduce myeloid progenitors and to induce MPD development in vivo.

DISCUSSION

In this study, we identified some of the mechanisms by which JunB regulates LT-HSC functions and elucidated how inactivation of this key transcription factor can lead to overproduction of myeloid progenitors and MPD development in vivo. We found that JunB normally controls LT-HSC proliferation and limits their

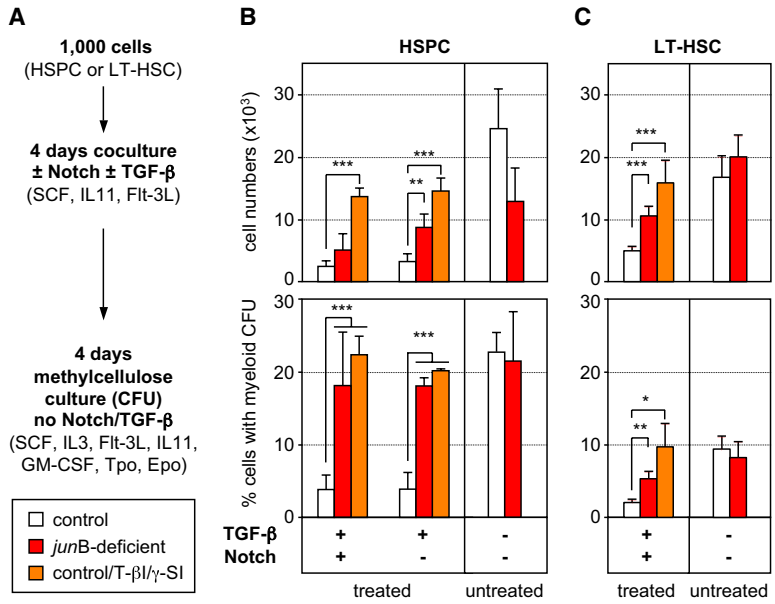

Figure 6. Defective Notch and TGF-β Pathway Responsiveness Contributes to the Overproduction of Myeloid Progenitors from *jun*B-Deficient LT-HSCs

(A) Schematic of the experimental design. Cells were directly sorted into 96-well plates (1,000 cells per well) containing OP9 (Notch$^-$) or OP9DL1 (Notch$^+$) cells and incubated for 4 days with or without 5 ng/ml TGF-β in the presence or absence of TGF-β inhibitor (T-βI; 5 μM) and γ-secretase inhibitor (γ-SI; 10 μM). Cells where then counted and replated in methylcellulose to determine the percentage of cells with myeloid colony-forming activity (CFU) present in each culture condition.

(B) Comparison between control and *jun*B-deficient HSPCs. The results shown are the averages ± SD of four independent experiments performed in duplicate (**$p \leq 0.01$, ***$p \leq 0.001$).

(C) Comparison between control and *jun*B-deficient LT-HSCs. The results shown are the averages ± SD of two independent experiments performed in triplicate (*$p \leq 0.05$, **$p \leq 0.01$, ***$p \leq 0.001$).

rate of production of myeloid progenitors by maintaining appropriate responsiveness to Notch and TGF-β signaling, in part through transcriptional regulation of *Hes1*, an important mediator of both pathways. These functions place JunB at the center of the complex network of cell-intrinsic and cell-extrinsic signals that ensure coordinated regulation of LT-HSC proliferation and differentiation, independently of LT-HSC maintenance and self-renewal activity. Taken together, our results provide a potential mechanism for disease initiation in the range of human myeloid malignancies in which *jun*B inactivation has already been reported (Yang et al., 2003; Steidl et al., 2006). Moreover, they expand our current understanding of the normal biology of the HSC compartment and the abnormal properties of HSC-derived LSCs.

Rethinking Transplantation Assays Used to Analyze HSC Number and Activity

HSCs have been defined and studied for many decades based on their ability to engraft and reconstitute the blood system of transplanted mice (Orkin and Zon, 2008). This functional property has allowed for the phenotypic identification and isolation of progressively more enriched HSC populations (Table S4). Hence, it has become common practice to enumerate HSCs by performing limiting dilution transplantation experiments with unfractionated BM cells. While this technique provides a valid assessment of HSC numbers in normal situations, our results demonstrate that it is a potentially unreliable method of determining HSC number and function in pathological situations. Hence, when we compared the same numbers of control and *jun*B-deficient unfractionated BM cells or enriched but not pure HSC populations (Flk2$^-$ LSK cells or HSPCs) side by side, we observed engraftment defects from *jun*B-deficient cells associated with deregulated cell-cycle distribution, loss of quiescence, and impaired serial transplantability by the third passage (data not shown). Only upon isolation of HSCs to near functional purity (using CD150$^+$/CD48$^-$/Flk2$^-$ LSK surface markers, one of the best phenotypic combinations currently available) did we uncover that *jun*B-deficient LT-HSCs had in fact normal engraftment capability as well as normal cell-cycle distribution, with more than 90% of the BM population quiescent at any given time. By using the same amount of unfractionated BM or partially purified HSPCs for both genotypes, we mistakenly injected fewer of the engrafting LT-HSCs and more of the overproduced nonengrafting differentiating cells for *jun*B-deficient populations than for control populations (Table S4). This dilution effect was also observed when we transplanted the quiescent fraction of the *jun*B-deficient HSPC compartment, as the expanded CD48$^+$/Flk2$^-$ LSK subset also displayed a large portion of quiescent cells (Figure S3). These results have at least two important implications. First, they demonstrate that quiescence per se is not a defining characteristic of LT-HSCs and should not be used as the sole criterion for identifying this cell population, even in an enriched subset. In fact, most of the early progenitor cells, including short-term hematopoietic stem cells and multipotent progenitors, have ≥50% of their population in the G_0 phase of the cell cycle at any given time (Passegué et al., 2005). Second, our results indicate that one must transplant a highly purified cell population when assessing LT-HSC numbers and properties in situations in which artificially introduced genetic alterations (in mice) or naturally occurring mutations (in humans) can affect the biological activity of the HSC compartment, leading to either overproduction or underproduction of differentiating cells. Incorrect assumptions may otherwise be made regarding the number and self-renewal activity of these mutant LT-HSCs.

Proliferation and HSC Maintenance

Several studies have suggested that increased HSC proliferation may lead to stem cell exhaustion and loss of maintenance in the BM microenvironment (Orford and Scadden, 2008). Here, we show that *jun*B-deficient LT-HSCs incorporate BrdU twice as fast as normal LT-HSCs due to direct or indirect changes in the regulation of their cell-cycle machinery (i.e., increases in *cyclin C* and *cyclin A2* expression and decreases in *cyclin D1*,

p18, and *p57* CKI levels) but do not display any changes in their BM numbers, quiescence status, engraftment, or regenerative potential in vivo. These results clearly demonstrate that HSC maintenance in the BM niches and self-renewal activity are not solely dictated by LT-HSC proliferation rate. One question raised by these observations is how nearly identical numbers of quiescent LT-HSCs can be maintained in the BM microenvironment in both control and *jun*B-deficient mice. One possibility is that *jun*B-deficient LT-HSCs could have shorter cell-cycle length, leading to increased turnover rates and BrdU accumulation without an increase in population size or decrease in G_0 frequency. Another possibility is that *jun*B-deficient LT-HSCs have increased proliferation (without changes in the length of their cell cycle) but that the overproduced LT-HSCs are displaced from the BM (perhaps due to lack of available niches) and released into the periphery, where they eventually become exhausted. This would imply the existence of retention mechanisms provided by the BM niches that would specifically maintain a preset number of quiescent LT-HSCs over an excess of cycling LT-HSCs. While such mechanisms are still poorly understood, they are likely to involve cell-cell and cell-matrix adhesion molecules such as α4/β1-VLA4 integrins, CD44, or CXCR4/SDF-1α, which are expressed on HSCs and are important for their retention in the BM. Increased numbers of functional LT-HSCs are found in the PB, liver, and spleen of *jun*B-deficient mice (unpublished data), which also develop pronounced extramedullary hematopoiesis (Passegué et al., 2004), suggesting that displacement of overproduced LT-HSCs might indeed be occurring in these mice as has already been found in other related mutant mice (Min et al., 2008).

Control of HSC Differentiation

Despite being extensively studied, the intricate molecular machinery and signaling mechanisms that coordinately regulate HSC proliferation and differentiation have remained largely elusive (Akala and Clarke, 2006; Blank et al., 2008). Here, we showed that at least two developmentally conserved signaling pathways that play a controversial role in HSC self-renewal (Notch and TGF-β) are in fact critical for limiting the rate at which HSCs produce myeloid progenitors. First, we found that the MPD-producing *jun*B-deficient LT-HSCs have impaired responsiveness to both Notch activation and TGF-β stimulation as measured by decreased induction of downstream effectors of these pathways (i.e., *Smad7*, *p57*, and *Hes1*). Second, using normal LT-HSCs and pharmacological inhibitors, we showed that impairing responsiveness to the TGF-β pathway in the presence of attenuated Notch stimulation leads to deregulated production of myeloid progenitors in vitro. Notch signaling has been shown to be necessary for maintaining HSCs in an undifferentiated state in the presence of proliferative signals in vitro (Duncan et al., 2005). Recently, it has been reported that the complete absence of canonical Notch signaling does not affect LT-HSC maintenance and self-renewal in vivo (Maillard et al., 2008). TGF-β is one of the most potent inhibitors of HSC growth in vitro (Sitnicka et al., 1996) and a negative regulator of myelopoiesis in vivo (Letterio and Roberts, 1998). Similar to Notch, it has been shown that absence of TGF-β signaling does not affect LT-HSC maintenance and self-renewal in vivo (Larsson et al., 2005). Taken together with our findings, these observations suggest that Notch and TGF-β belong to a complex network of signaling mechanisms provided by the BM niches that limit the rates at which LT-HSCs proliferate and produce myeloid progenitors without affecting their maintenance and self-renewal activity (see model in Figure 7A). In this context, JunB appears essential to maintain appropriate responsiveness to both Notch and TGF-β signaling due to its direct or indirect function in maintaining the expression levels of key downstream effectors of these pathways, including the *Hes1* gene. As a consequence, loss of JunB renders the HSC compartment refractory to these negative regulatory mechanisms, resulting in increased production of myeloid progenitors and MPD development in vivo.

Deconstructing the JunB Transcriptional Network in HSCs

Here, we have demonstrated that JunB is a core transcriptional regulator of HSC functions that controls a vast network of interconnected genes and pathways involved in numerous fate decisions including proliferation and early myeloid differentiation (see model in Figure 7B). We also identify *Hes1* as a direct JunB transcriptional target that could be involved in mediating part of these effects. However, direct or indirect deregulation of other effector genes including (but not limited to) *Hes5*, *Notch1*, *Pten*, *HoxB4*, and *HoxA9* is likely to play a role in establishing or maintaining the aberrant biological functions displayed by *jun*B-deficient HSPCs. Furthermore, it remains to be determined how loss of JunB results in the activation of LT-HSC cell-cycle machinery. JunB is a known transcriptional activator of *p16* (Passegué and Wagner, 2000) and a transcriptional repressor of both *cyclin D1* and *cyclin A* (Bakiri et al., 2000; Andrecht et al., 2002). While we did observe the expected increase in *cyclin A2* in *jun*B-deficient HSPCs, neither *p16* (unchanged) nor *cyclin D1* (decreased) behaved as predicted. It is possible that still uncharted changes in other transcriptional regulators and/or signaling pathways could counterbalance the direct effect of loss of JunB on the expression level of those genes. Alternatively, differences in JunB-mediated transcriptional regulation in distinct cell types (fibroblasts versus HSCs) or other confounding factors, such as the age of the mice, could explain these discrepancies. In fact, decreased *p16* expression is observed in *jun*B-deficient HSPCs isolated from older MPD mice (Passegué et al., 2004), consistent with an enhanced role for p16 in controlling the biology of aging HSCs (Janzen et al., 2006). Genome-wide ChIP analysis will be required to gain a better understanding of these complex regulations and further delineate the JunB transcription network in HSCs.

LSC Transformation

Our results indicate that deregulating the network of signaling mechanisms that control the balance between HSC proliferation and differentiation can lead to aberrant myeloid progenitor expansion and MPD development without causing LT-HSC exhaustion. These findings have important implications for understanding the development of myeloid malignancies in humans. They provide a mechanism to explain how mutations that increase the proliferation of a single LT-HSC can become dominant and lead to the expansion of an aberrant clone within the otherwise normal HSC compartment. They also explain how human LSCs emerging from the HSC compartment, such

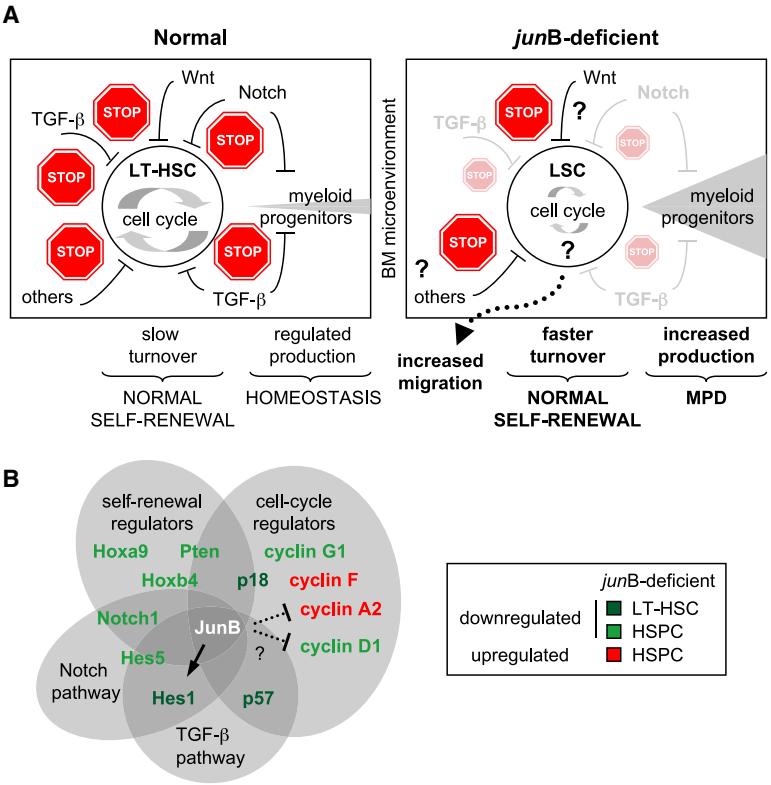

Figure 7. JunB Is a Key Transcriptional Regulator of the HSC Compartment that Controls LT-HSC Proliferation and Differentiation without Affecting Self-Renewal

(A) Model summarizing the defective regulation of *jun*B-deficient LT-HSCs. Normal LT-HSCs (left) in their BM microenvironment are maintained as slowly cycling, mostly quiescent cells due to the concerted action of a complex network of extrinsic regulatory pathways that provide multiple stop signals to limit proliferation and rates of myeloid progenitor production. In the absence of *jun*B expression (right), LT-HSCs lose responsiveness to at least two of these key negative regulatory pathways (Notch and TGF-β), leading to a dampening of the stop signals provided by the BM microenvironment. As a result, *jun*B-deficient LT-HSCs display increased turnover rates without overt expansion in the BM niches (most likely due to increased migration into the periphery) and overproduce myeloid progenitors, leading to MPD development in vivo. Importantly, *jun*B-deficient LT-HSCs have normal self-renewal potential, indicating that the mechanisms controlling LT-HSC maintenance are unaffected in these leukemia-initiating stem cells (LSCs).

(B) The JunB transcriptional network in hematopoietic stem and early progenitor cells. Lines (arrow = activation; blunted = inhibition) represent confirmed (solid) or unconfirmed (dotted) direct JunB transcriptional targets.

as in CML, can be maintained as a quiescent, self-renewing, nonexpanding population that overproduces myeloid progenitors and mature cells (Holyoake et al., 1999) and resists most current antileukemia treatments (Jordan et al., 2006). Similar to *jun*B-deficient LT-HSCs escaping 5-FU killing and regenerating the MPD in treated mice, CML LSCs might escape therapeutic treatment by taking advantage of the intact HSC-associated protection mechanisms provided by the BM niches. It is also tempting to speculate that BCR-ABL (the fusion oncoprotein encoded by the t(9;22) translocation, the hallmark of CML) might act very similarly to *jun*B inactivation by deregulating differentiation without affecting LT-HSC self-renewal mechanisms. It will be interesting to use the spectrum of deregulation observed in *jun*B-deficient HSCs as a road map to investigate *BCR-ABL*-expressing HSCs and determine whether similar pathways are affected. This type of comparison could uncover common deregulated mechanisms used by different oncogenic events and identify shared targets available for therapeutic intervention aimed at limiting LSCs' aberrant functional properties or preventing HSC transformation into LSCs.

EXPERIMENTAL PROCEDURES

Mice

Congenic C57BL/6-CD45.1 mice were used as donors (4–6 weeks old) for purification of wild-type cells and as recipients (8–12 weeks old) for transplantation experiments. Control and *jun*B-deficient (*jun*B$^{fl/fl}$MORE-*Cre*) C57BL/6-CD45.2 mice have been described previously (Passegué et al., 2004). β-actin-GFP C57BL/6-CD45.1 transgenic mice (Forsberg et al., 2006) were used as donors (4–6 weeks old) for purification of GFP-expressing competitor cells and to obtain, upon crossing, GFP-expressing control and *jun*B-deficient mice. 5-FU (150 mg/kg) was administrated by intraperitoneal injection. All animal experiments were performed in accordance with protocols approved by the University of California, San Francisco Institutional Animal Care and Use Committee.

Flow Cytometry

Cell preparation, staining, analysis, and isolation procedures were performed as described previously (Forsberg et al., 2006; Kiel et al., 2005). Additional information can be found in Table S5. After staining, cells were resuspended in Hank's buffered saline solution (HBSS) containing 2% heat-inactivated FBS (HyClone) and 1 μg/ml propidium iodide for dead cell exclusion and were sorted on a FACSAria or analyzed on a LSR II (Becton Dickinson). Each subpopulation was double sorted and reanalyzed to ensure maximum purity.

Transplantations

Congenic recipient mice were irradiated using a cesium source irradiator with lethal (1200 rad) or sublethal (950 rad) doses delivered in a split dose 3 hr apart and were given antibiotic-containing water for at least 6 weeks postirradiation. For in vivo homing experiments, mice were irradiated 1 day prior to injections. For all other transplantation experiments, mice were injected immediately after irradiation. For intravenous injections, cells were resuspended in a volume of 100 μl and injected into the retro-orbital plexus. For intrafemoral injections, cells were resuspended in a volume of 30 μl and injected through the knee into the femoral cavity of anesthetized mice. Donor and recipient cells were distinguished by expression of GFP or different allelic forms of CD45 (CD45.1 versus CD45.2).

Cell Cycle and Intracellular Staining

Short- and long-term BrdU kinetics as well as live Hoechst 33342 (H)/pyronin Y (PY) staining were performed as described previously (Passegué et al., 2005; Kiel et al., 2007) (Table S5). Intracellular 7-aminoactinomycin D (7AAD)/PY and cyclin D1 staining of unfractionated BM cells were performed as described in Table S5.

Gene Expression Analysis

Total RNA was isolated using TRIzol reagent (Invitrogen), digested with DNase I, and used for reverse transcription according to the manufacturer's instructions (SuperScript III kit, Invitrogen). qRT-PCR primers were designed using Primer Express software (Applied Biosystems) (Table S6). All reactions were performed in an ABI 7300 sequence detection system using SYBR Green PCR Core reagents (Applied Biosystems) and cDNA equivalent of 200 cells per reaction as described previously (Forsberg et al., 2006). Expression levels of β-*actin* or ribosomal protein L-19 (*RL-19*) genes were used to normalize the amount of the investigated transcripts.

Cell Cultures

Hematopoietic cocultures were performed in Iscove's modified Dulbecco's medium (IMDM) containing 5% FBS, 1× penicillin/streptomycin, 2 mM GlutaMax-1, 0.1 mM nonessential amino acids, 1 mM sodium pyruvate, and 50 μM 2-mercaptoethanol and supplemented with 25 ng/ml of SCF, Flt3-L, and IL11. For coculture experiments, HSCs were sorted directly over a monolayer of OP9 and OP9DL1 cells plated in a 96-well plate (5,000–20,000 cells per well) and grown for up to 4 days (with medium addition every 2 days) with or without 5 ng/ml recombinant human TGF-β1 (R&D Systems), 10 μM γ-secretase inhibitor (XXI; Calbiochem), and/or 5 μM TGF-β inhibitor (SB431542; Sigma). Following the culture period, HSC-derived cells were collected, transferred in a 96-well plate, incubated for 20 min at 37°C to deplete for contaminating stromal cells, re-collected, rinsed once with HBSS, and then either resuspended in TRIzol reagent for RNA isolation or counted, diluted (1:3 to 1:50), and replated in methylcellulose. Myeloid colony-forming activity was evaluated after 4 days of culture in IMDM-based methylcellulose medium (M3231; Stem Cell Technologies) supplemented with SCF (25 ng/ml), Flt3-L (25 ng/ml), IL-11 (25 ng/ml), IL-3 (10 ng/ml), Tpo (25 ng/ml), Epo (4 U/ml), and GM-CSF (10 ng/ml).

Statistical Analysis

p values were calculated using Student's unpaired t test.

SUPPLEMENTAL DATA

The Supplemental Data include Supplemental Experimental Procedures, Supplemental References, six tables, and five figures and can be found with this article online at http://www.cancercell.org/supplemental/S1535-6108(09)00072-5.

ACKNOWLEDGMENTS

We thank A. Wagers, D. Laird, and R. Blelloch for critical reading of the manuscript; J. Stuart for bioinformatics assistance; and M. Dail for assistance with the Notch experiments. M.S. is supported by a fellowship from Fonds de la recherche en santé du Québec, and K.S. is supported by a Rubicon grant from the Netherlands Organisation for Scientific Research (NWO) and a fellowship from the Dutch Cancer Society (KWF). E.C.F. is the recipient of a California Institute for Regenerative Medicine New Investigator Award, and B.S.B. and E.P. are recipients of American Society of Hematology Scholar Awards. This work was supported by research grants from the Concern Foundation and the UCSF Research Evaluation and Allocation Committee, a shared V Foundation Translational Award, and NIH grant HL092471 to E.P.

Received: July 26, 2008
Revised: December 18, 2008
Accepted: February 12, 2009
Published: April 6, 2009

REFERENCES

Akala, O.O., and Clarke, M.F. (2006). Hematopoietic stem cell self-renewal. Curr. Opin. Genet. Dev. *16*, 496–501.

Andrecht, S., Kolbus, A., Hartenstein, B., Angel, P., and Schorpp-Kistner, M. (2002). Cell cycle promoting activity of JunB through cyclin A activation. J. Biol. Chem. *277*, 35961–35968.

Bakiri, L., Lallemand, D., Bossy-Wetzel, E., and Yaniv, M. (2000). Cell cycle-dependent variations in c-Jun and JunB phosphorylation: a role in the control of cyclin D1 expression. EMBO J. *19*, 2056–2068.

Blank, U., Karlsson, G., and Karlsson, S. (2008). Signaling pathways governing stem-cell fate. Blood *111*, 492–503.

Blokzijl, A., Dahlqvist, C., Reissmann, E., Falk, A., Moliner, A., Lendahl, U., and Ibáñez, C.F. (2003). Cross-talk between the Notch and TGF-beta signaling pathways mediated by interaction of the Notch intracellular domain with Smad3. J. Cell Biol. *163*, 723–728.

Cheshier, S.H., Morrison, S.J., Liao, X., and Weissman, I.L. (1999). In vivo proliferation and cell cycle kinetics of long-term self-renewing hematopoietic stem cells. Proc. Natl. Acad. Sci. USA *96*, 3120–3125.

Duncan, A.W., Rattis, F.M., DiMascio, L.N., Congdon, K.L., Pazianos, G., Zhao, C., Yoon, K., Cook, J.M., Willert, K., Gaiano, N., et al. (2005). Integration of Notch and Wnt signaling in hematopoietic stem cell maintenance. Nat. Immunol. *6*, 314–322.

Forsberg, E.C., Serwold, T.C., Kogan, S., Weissman, I.L., and Passegué, E. (2006). New evidence supporting megakaryocyte-erythrocyte potential of Flk2/Flt3^{+} multipotent hematopoietic progenitors. Cell *126*, 415–426.

Holyoake, T., Jiang, X., Eaves, C., and Eaves, A. (1999). Isolation of a highly quiescent subpopulation of primitive leukemic cells in chronic myelogenous leukemia. Blood *94*, 2056–2064.

Janzen, V., Forkert, R., Fleming, H.E., Saito, Y., Waring, M.Y., Dombkowski, D.M., Cheng, T., DePinho, R.A., Sharpless, N.E., and Scadden, D.T. (2006). Stem-cell ageing modified by the cyclin-dependent kinase inhibitor p16INK4a. Nature *443*, 421–426.

Jin, L., Hope, K.J., Zhai, Q., Smadja-Joffe, F., and Dick, J.E. (2006). Targeting of CD44 eradicates human acute myeloid leukemic stem cells. Nat. Med. *12*, 1167–1174.

Jordan, C.T., Guzman, M.L., and Noble, M. (2006). Cancer stem cells. N. Engl. J. Med. *355*, 1253–1261.

Kiel, M.J., and Morrison, S.J. (2008). Uncertainty in the niches that maintain haematopoietic stem cells. Nat. Rev. Immunol. *8*, 290–301.

Kiel, M.J., Yilmaz, O.H., Iwashita, T., Yilmaz, O.H., Terhorst, C., and Morrison, S.J. (2005). SLAM family receptors distinguish hematopoietic stem and progenitor cells and reveal endothelial niches for stem cells. Cell *121*, 1109–1121.

Kiel, M.J., He, S., Ashkenazi, R., Gentry, S.N., Teta, M., Kushner, J.A., Jackson, T.L., and Morrison, S.J. (2007). Haematopoietic stem cells do not asymmetrically segregate chromosomes or retain BrdU. Nature *449*, 238–242.

Lapidot, T., Dar, A., and Kollet, O. (2005). How do stem cells find their way home? Blood *106*, 1901–1910.

Larsson, J., Blank, U., Klintman, J., Magnusson, M., and Karlsson, S. (2005). Quiescence of hematopoietic stem cells and maintenance of the stem cell pool is not dependent on TGF-beta signaling in vivo. Exp. Hematol. *33*, 592–596.

Letterio, J.J., and Roberts, A.B. (1998). Regulation of immune responses by TGF-beta. Annu. Rev. Immunol. *16*, 137–161.

Maillard, I., Koch, U., Dumortier, A., Shestova, O., Xu, L., Sai, H., Pross, S.E., Aster, J.C., Bhandoola, A., Radtke, F., et al. (2008). Canonical Notch signaling is dispensable for the maintenance of adult hematopoietic stem cells. Cell Stem Cell *2*, 356–366.

Min, I.M., Pietramaggiori, G., Kim, F.S., Passegué, E., Stevenson, K.E., and Wagers, A.J. (2008). The transcription factor EGR1 controls both the proliferation and localization of hematopoietic stem cells. Cell Stem Cell *2*, 380–391.

Orford, K.W., and Scadden, D.T. (2008). Deconstructing stem cell self-renewal: genetic insights into cell-cycle regulation. Nat. Rev. Genet. *9*, 115–128.

Orkin, S.H., and Zon, L.I. (2008). Hematopoiesis: an evolving paradigm for stem cell biology. Cell *132*, 631–644.

Osawa, M., Hanada, K., Hamada, H., and Nakauchi, H. (1996). Long-term lymphohematopoietic reconstitution by a single CD34-low/negative hematopoietic stem cell. Science *273*, 242–245.

Passegué, E., and Wagner, E.F. (2000). JunB suppresses cell proliferation by transcriptional activation of p16(INK4a) expression. EMBO J. *19*, 2969–2979.

Passegué, E., Jochum, W., Schorpp-Kistner, M., Möhle-Steinlein, U., and Wagner, E.F. (2001). Chronic myeloid leukemia with increased granulocyte progenitors in mice lacking JunB expression in the myeloid lineage. Cell *104*, 21–32.

Passegué, E., Wagner, E.F., and Weissman, I.L. (2004). JunB deficiency leads to a myeloproliferative disorder arising from hematopoietic stem cells. Cell *119*, 431–443.

Passegué, E., Wagers, A.J., Guiriato, S., Anderson, W., and Weissman, I.L. (2005). Global analysis of proliferation and cell cycle gene expression in the regulation of hematopoietic stem and progenitor cell fates. J. Exp. Med. *202*, 1599–1611.

Sitnicka, E., Ruscetti, F.W., Priestley, G.V., Wolf, N.S., and Bartelmez, S.H. (1996). Transforming growth factor beta 1 directly and reversibly inhibits the initial cell divisions of long-term repopulating hematopoietic stem cells. Blood *88*, 82–88.

Steidl, U., Rosenbauer, F., Verhaak, R.G., Gu, X., Otu, H.H., Klippel, S., Steidl, C., Bruns, I., Costa, D.B., Wagner, K., et al. (2006). Essential role of Jun family transcription factors in PU.1 knockdown-induced leukemic stem cells. Nat. Genet. *38*, 1269–1277.

Wang, J.C., and Dick, J.E. (2005). Cancer stem cells: lessons from leukemia. Trends Cell Biol. *15*, 494–501.

Yang, M.Y., Liu, T.C., Chang, J.G., Lin, P.M., and Lin, S.F. (2003). JunB gene expression is inactivated by methylation in chronic myeloid leukemia. Blood *101*, 3205–3211.